

# Response characteristics and suppression of torsional vibration of rectangular prisms with various width-to-depth ratios

Kazunori Takai<sup>†</sup> and Hiroshi Sakamoto<sup>‡</sup>

*Department of Mechanical Engineering, Kitami Institute of Technology,  
165 Koen-cho, Kitami, Hokkaido, 090-8507, Japan*

*(Received January 14, 2005, Accepted November 8, 2005)*

**Abstract.** The response characteristics and suppression of flow-induced vibrations of rectangular prisms with various width-to-depth ratios were experimentally investigated. The prisms were rigid and elastically mounted at both ends to enable constrained torsional vibrations only. The present study focused on torsional vibrations, one of the three types of flow-induced vibrations generated in a rectangular prism. First, the response characteristics of torsional vibrations generated in rectangular prisms were investigated by free-vibration tests. It was found that the response characteristics of torsional vibrations generated in rectangular prisms could be classified into six patterns depending on the width-to-depth ratio. Next, the response characteristics of torsional vibrations observed in the free-vibration tests were reproduced by forced-vibration tests, and the mechanisms by which the three types of flow-induced vibrations, low-speed torsional flutter, vortex excitation and high-speed torsional flutter, are generated in the rectangular prisms were elucidated on the basis of characteristics of fluid forces and visualized flow patterns. Experiments were also carried out to establish an effective method for suppressing flow-induced vibrations generated in the rectangular prisms, and it was found that low-speed torsional flutter and high-speed torsional flutter could be suppressed by placing a small normal plate upstream of the prism, which results in suppression of the alternating rolling-up of the shear layers separating from the leading edges of the prism. It was also found that vortex excitation could be suppressed by placing a splitter plate downstream of the prism, which results in suppression of the generation of wake vortices.

**Keywords:** rectangular prism; width-to-depth ratio; torsional vibration; suppression; control normal plate.

---

## 1. Introduction

Flow-induced vibrations are considered to be major problems in various areas of engineering because an aerodynamic instability vibrations phenomenon is experienced in various structures. For example, flow-induced vibrations of a structure in a flow are often seen as the possible cause of fatigue failure, as was seen in an accident involving the thermometer in a well of the fast breeder reactor “Monju” in 1995 at Japan. Therefore, the insight of problem on flow-induced vibrations phenomenon of the structures is still obscure. Many studies on flow-induced vibrations have been

---

<sup>†</sup> Research Assistant, Corresponding Author, E-mail: [takai@mech.kitami-it.ac.jp](mailto:takai@mech.kitami-it.ac.jp)

<sup>‡</sup> Professor, E-mail: [sakamoto@mech.kitami-it.ac.jp](mailto:sakamoto@mech.kitami-it.ac.jp)

carried out using a circular cylinder and a rectangular prism as representative structures. However, many points including the mechanism by which flow-induced vibrations are generated, are still not clear. Since the generation mechanism and response characteristics of flow-induced vibrations differ depending on the cross-sectional shape, there are many problems on the rectangular prism in comparison with those on the circular cylinder, which should reach to a solution. Flow-induced vibrations of a rectangular prism, particularly the response characteristics of an elastically supported rectangular prism, have been examined by various researchers. Shiraishi and Matsumoto (1983) examined the vortex excitation of the geometrical shape factor of the section. Nakamura and Nakashima (1986) examined the excitation measurements on spring-supported prisms with width-to-depth ratios ranging from 2.0 to 5.0. The vortex excitation and galloping generated rectangular prism with various width-to-depth ratios was discussed by Nakamura and Hirata (1994). However, there has been little investigation of the suppression and generation mechanism of flow-induced vibrations. Some reports to be noticed have been made on the generation mechanism of flow-induced vibrations of the rectangular prism. Matsumoto, *et al.* (1996, 1997) performed forced vibration tests to obtain an insight into the mechanisms underlying the generation of torsional vibration of two-dimensional rectangular prisms. Based on measurements of fluctuating pressure and phase lag between fluctuating pressure and the response of the prism, they showed that for a prism's width-to-depth ratio ( $B/H$ ) in the range of 5 to 12.5, the torsional flutter at low reduced velocity ( $U_r < 8$ ) is mainly due to convection of vortices along the side surfaces of the prism. For  $B/H=2.0$ , they found that flutter is mainly due to the action of fluid pressure force on the leeward part of the side surface and is controlled by the phase difference between separated flow from the leading edge and torsional response. Nakamura and Matsukawa (1987) clarified the relationship between flow-induced vibrations and fluctuating lift forces. Komatsu and Kobayashi (1980) examined the relationship between the response characteristics and the separated shear layer. Deniz and Staubli (1997) examined the relationship between wake vortices and the response characteristics. Tamura and Dias (2003) examined on unstable aerodynamic phenomenon of a rectangular prism with small side ratio and clarified pressure on the side surface of freely oscillating rectangular prism and the phase lag of pressure to the oscillation. Moreover, Itoh and Tamura (2002) and Leonard and Roshko (2001) examined the effects of mass ratio on response of unstable oscillation of a rectangular prism. A study on the suppression of galloping by installing ribs or flat plates on the surfaces of a rectangular prism was carried out by Naudascher, *et al.* (1981). Munshi, *et al.* (1997) controlled flow-induced vibrations by rotation of rotors installed at the corners of a rectangular prism. However, the generation of flow-induced vibrations of the rectangular prism could not be completely prevented in those studies. The authors (2000) showed that the generation of flow-induced vibrations could be almost completely suppressed by placing a T-shaped plate upstream of a rectangular prism having width-to-depth ratio of 3. However, it was not determined whether the use of a T-shaped plate placed upstream of the prism can prevent flow-induced vibrations of rectangular prisms with other width-to-depth ratios.

In this study, the response characteristics and the suppression of flow-induced vibrations of elastically mounted rectangular prisms in a steady flow were investigated. The flow around a rectangular prism can be classified into three patterns by the width-to-depth ratio  $B/H$  ( $B$ : width of the prism in the stream-wise direction,  $H$ : depth (thickness) of the prism in the direction normal to the flow), i.e., separated shear layer flow pattern ( $B/H < 3$ ) (Naudascher and Wang 1993), unsteady shear layer reattachment flow pattern ( $3 < B/H < 6$ ), and steady reattachment flow pattern ( $B/H > 6$ ) (Takeuchi and Matsumoto 1992). In the present study, rectangular prisms having various width-to-depth ratios ( $B/H=0.3\sim 8.6$ ) at which the three patterns of flow occur were used. Flow-induced vibrations of

rectangular prisms include cross-flow vibration in which the prism vibrates in the direction normal to the flow, in-line vibration in which the prism vibrates in the stream-wise direction, and torsional vibration in which the prism oscillates with an angular displacement. The present study focused on flow-induced torsional vibrations of prisms, one of the three possible types of flow-induced vibration described above. First, response characteristics were examined by free-vibration tests of elastically supported prisms. Next, the flow-induced vibrations observed in the free-vibration tests were reproduced by forced-vibration tests, and aerodynamic characteristics of the rectangular prisms, behavior of the shear layer that has separated from the leading edge, wake vortices and characteristics of impinging leading-edge vortices that induce flow-induced vibrations for certain cases were examined. The mechanism by which flow-induced vibrations are generated was also examined on the basis of the results. In addition, response characteristics were examined for the case in which a small normal plate is centrally placed upstream of the prism and for the case in which a splitter plate is placed downstream of the prism in order to suppress flow-induced vibrations. On the basis of the results, an effective method for suppressing flow-induced vibrations of rectangular prisms was established.

## 2. Parameters to be included

There are eight parameters that govern the angular displacement  $\alpha$  of torsional vibration of rectangular prisms having various width-to-depth ratios, i.e., the depth of the prism  $H$ , the width of the prism  $B$ , the approach velocity  $U$ , the density of the fluid  $\rho$ , viscosity of fluid  $\mu$ , the natural frequency (free damped torsional vibration) of the prism  $f_c$ , the mass moment of inertia per unit length of the prism  $I$  and the logarithmic decrement of damping  $\delta$ . Therefore, the functional relationship for the angular displacement  $\alpha$  of torsional vibration of the prism can be written as

$$\alpha = \varphi(H, B, U, \rho, f_c, I, m, \delta) \quad (1)$$

The above equation can be reduced to

$$\alpha = \varphi(\pi_1, \pi_2, \pi_3, B/H, \delta) \quad (2)$$

by choosing  $H$ ,  $U$  and  $\rho$  as the repeating variables:

$$\pi_1 = H^{\alpha_1} U^{\beta_1} \rho^{\gamma_1} f_c,$$

$$\pi_2 = H^{\alpha_2} U^{\beta_2} \rho^{\gamma_2} I,$$

$$\pi_3 = H^{\alpha_3} U^{\beta_3} \rho^{\gamma_3} \mu.$$

From the solutions of  $\pi_1 = f_c H/U$ ,  $\pi_2 = I/(H^4 \rho)$  and  $\pi_3 = \mu/(HU\rho)$  from the above three equations, Eq. (2) can be written as

$$\begin{aligned} \alpha &= \varphi\left(\frac{f_c H}{U}, \frac{I}{H^4 \rho}, \frac{\mu}{HU\rho}, \frac{B}{H}, \delta\right) \\ &= \varphi\left(\frac{U}{f_c H}, \frac{I\delta}{H^4 \rho}, \frac{HU\rho}{\mu}, \frac{B}{H}\right). \end{aligned} \quad (3)$$

By introducing the reduced velocity  $U_r = U/(f_c H)$ ,  $Cn = I\delta/\rho H^4$ , and  $Re = HU\rho/\mu$ , Eq. (3) becomes

$$\alpha = \varphi(U_r, Cn, Re, B/H).$$

Here, the angular displacement  $\alpha$  and the reduced mass-damping parameter  $Cn$  are independent on  $Re$ . Moreover, the reduced velocity  $U_r$  includes  $Re$  since  $U_r$  is a function of  $Re$ . Therefore, we can adopt a non-dimensional parameter either  $U_r$  or  $Re$ . In this study,  $U_r$  usually used in handling flow-induced vibrations is adopted. Thus,  $Re$  can be dropped from the above equation:

$$\alpha = \varphi(U_r, Cn, B/H) \quad (4)$$

Therefore, the angular displacement  $\alpha$  is governed by three non-dimensional parameters, i.e., the reduced velocity  $U_r$ , the reduced mass-damping parameter  $Cn$  and the width-to-depth ratio  $B/H$ .

### 3. Experimental setups and procedures

Both free-vibration and forced-vibration tests were performed in the present study. Here free-vibration means vibration of an elastically mounted prism in a steady flow. In the forced-vibration tests, the characteristics of fluctuating pressures and aerodynamic forces acting on the rectangular prisms were investigated by using a low-speed Eiffel-type wind tunnel. The test section of the wind tunnel was rectangular in shape with a depth of 1.0 m, a width of 0.35 m, and a length of 2.0 m. The prism used in the forced-vibration tests had various widths with a depth of 100 mm. The prism had many piezometric holes to measure the fluctuating pressure distributions on the surfaces, as shown in Fig. 1. The piezometric holes were connected to a semiconductor pressure transducer installed inside the prism. The pressure transducer was set up in a hollow pipe in order to eliminate the effects of vibration transmitted from the prism. When the pressure transducer was connected to the piezometric holes, it responded to pressure fluctuation up to 100 Hz with a gain factor of  $1 \pm 0.05$ , the phase lag being negligible. The aerodynamic forces were estimated from the ensemble-averaged fluctuating pressures. The prism was forced into torsional vibration at an angular displacement ranging from  $0^\circ$  to  $\pm 5^\circ$ . In the tests, the reduced velocity  $U_r$  [ $=U/(f_c H)$ , where  $U$  is the free-stream velocity,  $H$  is the depth of the prism, and  $f_c$  is the natural frequency of the prism] was varied from 2.5 to 40. The corresponding Reynolds number  $Re$  ( $=UH/\nu$ ) was  $2.65 \times 10^4$  to  $7.28 \times 10^4$ .

The free-vibration tests were carried out in a low-speed, closed-circuit wind tunnel. The test section of the wind tunnel was rectangular in shape with a width of 0.3 m, a height of 1.2 m, and a length of 2.5 m. The width-to-depth ratio of the tested prism was changed from 0.3 to 8.6, as shown

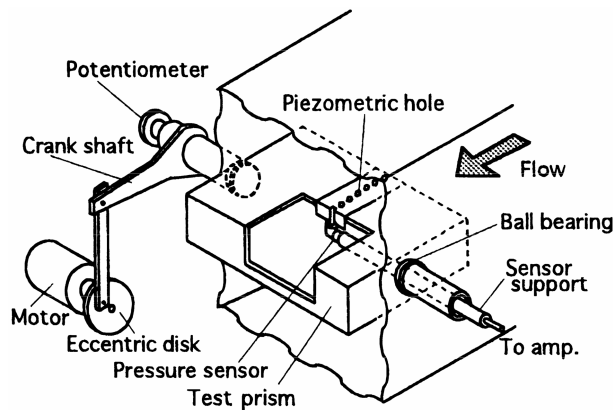


Fig. 1 View of forced-vibration experimental equipment

Table 1 Values of critical reduced velocity  $U_{rc}$ , natural frequency  $f_c$ , logarithmic decrement of damping  $\delta$  and reduced mass-damping factor  $Cn$  adopted in the present study

$B/H$	$U_{rc}$	$f_c$	$\delta$	$Cn$	$B/H$	$U_{rc}$	$f_c$	$\delta$	$Cn$
0.3	6.13	9.8	0.014	7.580	2.7	6.80	5.9	0.010	0.027
0.4	6.25	9.8	0.010	2.057	2.8	6.94	5.9	0.009	0.023
0.5	6.76	9.8	0.011	0.895	3.0	6.78	6.8	0.014	0.020
0.7	7.09	9.2	0.010	0.300	3.5	7.03	4.7	0.016	0.030
1.0	7.35	9.4	0.019	0.233	3.6	7.30	5.5	0.038	0.047
1.1	7.09	9.0	0.010	0.132	3.7	7.41	5.3	0.045	0.051
1.2	7.25	8.8	0.011	0.125	4.0	7.77	5.5	0.017	0.016
1.3	7.63	8.4	0.010	0.104	4.5	8.26	4.1	0.020	0.021
1.5	8.47	9.0	0.017	0.086	5.0	9.31	3.7	0.015	0.010
1.6	8.85	8.4	0.014	0.091	5.6	9.63	8.2	0.011	0.009
1.7	8.85	8.8	0.016	0.026	6.0	7.73	8.2	0.023	0.011
1.8	9.90	7.4	0.010	0.055	6.6	7.35	7.4	0.021	0.010
2.0	11.69	8.2	0.011	0.032	7.0	6.89	9.4	0.004	0.002
2.2	13.33	7.8	0.012	0.035	7.6	6.57	9.6	0.027	0.011
2.4	14.93	7.6	0.011	0.023	8.0	6.58	8.6	0.022	0.009
2.6	16.67	6.4	0.011	0.028	8.6	6.58	7.8	0.019	0.007

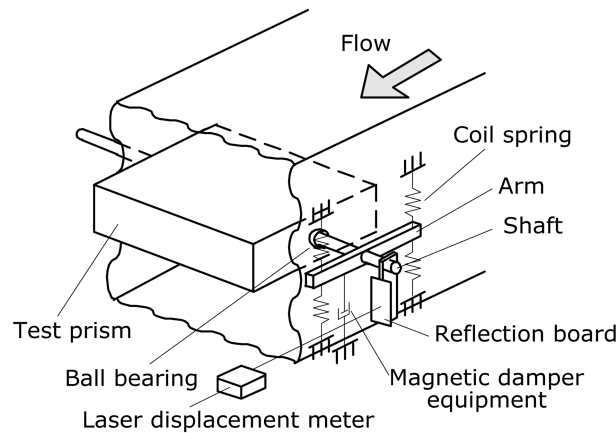


Fig. 2 View of free-vibration experimental equipment

in Table 1. The depth of the prism used in each test was 100 mm. The prism was supported by four coil springs attached to the outside of the wind tunnel, as shown in Fig. 2, enabling torsional vibration of the prism. Also, the reduced mass-damping factor  $Cn$  ( $=I\delta/\rho B^4$ , where  $I$  is the inertia moment per unit length of prism,  $\delta$  is the logarithmic decrement of damping, and  $\rho$  is the density of fluid) was changed using two magnetic dampers. The response characteristics of torsional vibration of the prism were investigated by varying the reduced velocity  $U_r$  from 1 to 35 for the plain prisms and the controlled prisms. The flow-induced vibrations were suppressed by the use of a normal plate and a splitter plate placed upstream and downstream of the prism, respectively, as shown in Fig. 3(b) and (c). The angular displacement and oscillation frequency of the prism were measured

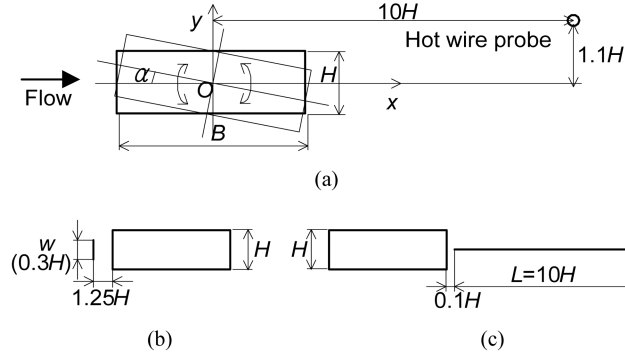


Fig. 3 Coordinate system and definition of symbols: (a) plain prism, (b) normal plate set-up, and (c) splitter plate set-up

using a laser-displacement meter. Table 1 shows values of critical reduced velocity  $U_{rc}$ , natural frequency  $f_c$ , logarithmic decrement of damping  $\delta$  and reduced mass-damping factor  $Cn$  adopted in the free-vibration tests. The corresponding Reynolds number in the free-vibration tests was  $6.6 \times 10^3$  to  $9.9 \times 10^4$ . Also, flow patterns in a recirculating water channel with a test section of 30 cm in width, 40 cm in depth and 2 m in length were observed by uranine dye, which was injected from two holes, each with a diameter of 1 mm, located on the upper and lower sides in the neighborhood of the leading edge of the prism. Flow patterns generated at a constant free-stream velocity of  $U=0.8$  cm/s, corresponding to a Reynolds number of about 350, were observed. The amplitude of oscillation of the prisms during flow visualization tests was varied from  $0^\circ$  to  $\pm 5^\circ$ .

## 4. Results and discussion

### 4.1. Response characteristics of torsional vibration of rectangular prisms

Fig. 4 shows values of the Strouhal number  $St (=f_n H/U)$ , i.e., the nondimensional frequency of vortex shedding for stationary rectangular prisms with various width-to-depth ratios ( $B/H$ ) ranging from 0.3 to 8.6. The values of  $St$  corresponding to different values of  $B/H$  are almost the same as those reported previously (Okajima, *et al.* 1980, Nakaguchi, *et al.* 1968, Otuki, *et al.* 1974, Sakamoto, *et al.* 1989); that is, drastic changes in  $St$  are seen in the neighborhood of  $B/H=3.0$ , at which the separated shear layer flow pattern changes to an unsteady reattachment flow pattern, and in the neighborhood of  $B/H=6.0$ , at which the unsteady reattachment flow pattern changes to a steady reattachment flow pattern. The reduced critical velocity  $U_{rc} (=U/(f_n H))$  used in the present experiments is the reciprocal of  $St$  shown in Fig. 4. Note that here calculation of the Strouhal number was based on the depth of the prism, as opposed to the width adopted by some researchers. When the width of the prism is chosen as the characteristic length dimension to calculate Strouhal numbers, the values of Strouhal numbers become a constant of 0.6 for the range of  $B/H=3\sim 6$  (Mills, *et al.* 2003).

Fig. 5 shows the response characteristics of each type of flow-induced vibrations of prisms with different  $B/H$  ratios. The ordinate axis shows the rms value of angular displacement  $\alpha$  of torsional vibration, and the abscissa shows the reduced velocity  $U_r$ . The results are shown as a representative pattern in each of the response characteristics, which could be classified into six patterns depending on the width-to-depth ratio of the prism. As shown in Fig. 5(a), only vortex excitation (abbreviated hereafter as VE) occurs in the case of prisms with  $B/H$  ratios up to 1.1, and the VE is a limited

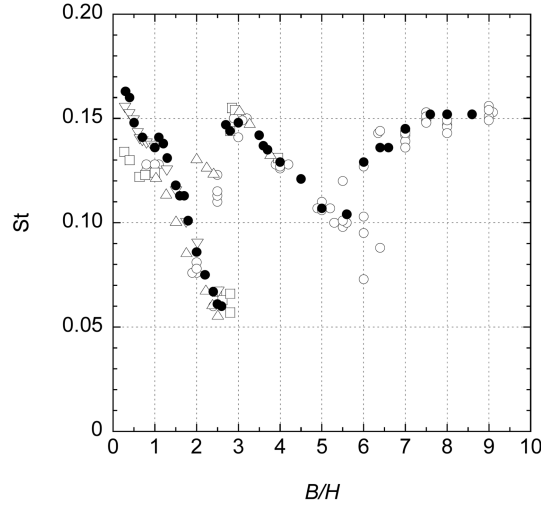


Fig. 4 Distributions of Strouhal number  $St$  in response to change in  $B/H$ :  $\circ$ , Okajima, *et al.*;  $\square$ , Nakaguchi, *et al.*;  $\triangle$ , Otsuki, *et al.*;  $\nabla$ , Sakamoto, *et al.*;  $\bullet$ , present study

excitation that becomes convergent. VE, as is described in detail in section 4.3, is generated by fluctuating pressures acting on the surfaces of the prism, which are caused by alternating rolling-up of the shear layer separating from the leading edge of the prism in synchronization with the generation of Kármán vortices behind the prism. Since the fluctuating pressures acting on the surfaces of the prism are asymmetric with respect to the  $x$ -axis and  $y$ -axis, which are the central axes of the prism, a fluctuating moment is generated with respect to the central axes and then induces torsional vibration. As shown in Fig. 5(b), for prisms with  $B/H$  ratios ranging from 1.2 to 1.6, VE diverges without converging. However, VE converges when the reduced mass-damping factor  $Cn$  is increased. From a phenomenological point of view, there is no basic difference between the response characteristics of patterns 1 and 2 except for the effect of  $Cn$ , because if a smaller value of  $Cn$  is applied on the prisms of pattern 1, its VE should be divergent. Hence, pattern 1 seems to be identical to pattern 2. As shown in Fig. 5(c), for prisms with  $B/H$  ratios ranging from 1.7 to 2.6, low-speed torsional flutter (abbreviated hereafter as LSTF) and high-speed torsional flutter (abbreviated hereafter as HSTF) are generated. The LSTF that is generated at low  $U_r$  is caused by the reattachment of some of the shear layer separating from the leading edge of the prism to the side surfaces of the prism. In the case of the HSTF, the shear layer separating from the leading edge of the prism does not reattach to the side surface of the prism but rolls up behind the prism, and this rolling-up of the separated shear layer behind the prism causes the HSTF. It is notable that HSTF can be generated at values of  $U_r$  lower than those at which VE occurs and becomes a divergent vibration as can be seen when  $B/H=2.0$ . It should be noted that Takeuchi and Matsumoto (1992) found LSTF and high-speed divergent torsional flutter for  $B/H=2.0$ ; however, they did not find any torsional vibration for  $B/H=1.0$  and  $0.5$ . The disappearance of torsional vibration for  $B/H=1.0$  and  $0.5$  in their experiment can be attributed to a higher value of  $Cn$  than that in the present experiments. As shown in Fig. 5(d), for prisms with  $B/H$  ratios ranging from 2.7 to 3.6, three types of flow-induced vibrations, LSTF, VE and HSTF, are generated. The LSTF, as is described in detail later, is induced by the impinging leading-edge vortices that are generated on the side surfaces of the prism, and the LSTF is generated at about half of the value of  $U_{rc}$  at which the VE begins to

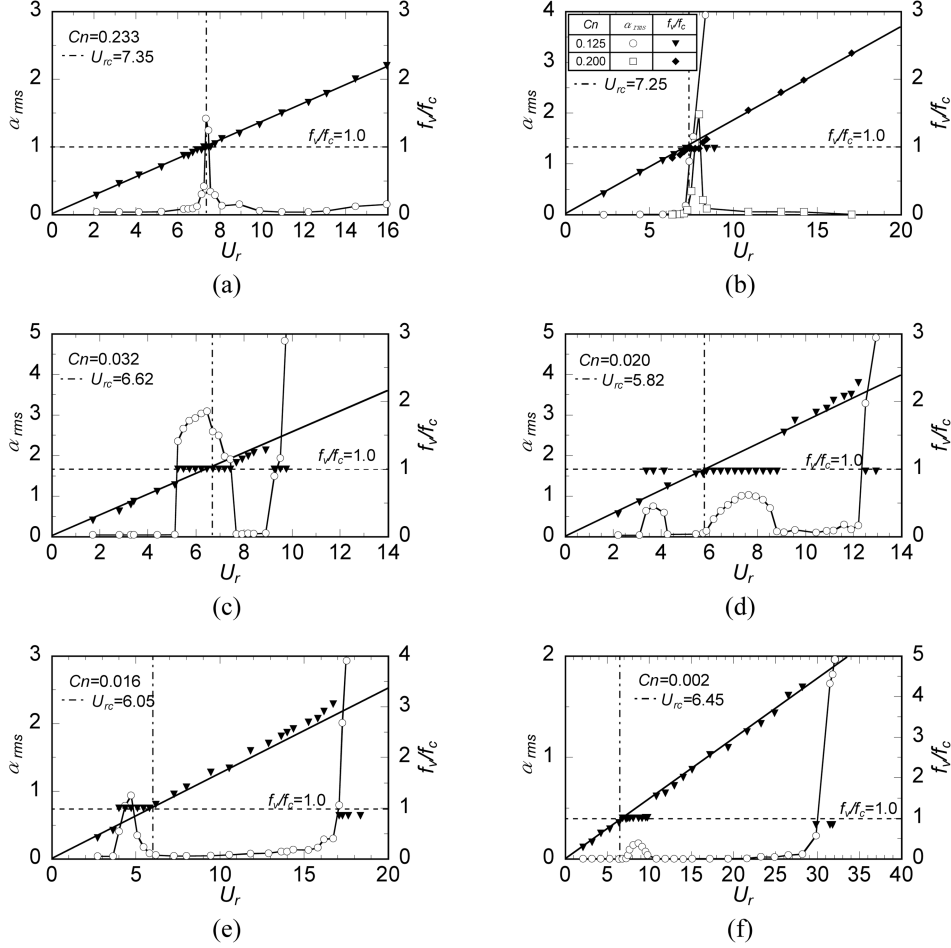


Fig. 5 Response characteristics of rotary oscillation of prisms: ○,  $\alpha_{rms}$ , ▼,  $f_v/f_c$ ; (a)  $B/H=1.0$  (pattern 1); (b)  $B/H=1.2$  (pattern 2); (c)  $B/H=2.0$  (pattern 3); (d)  $B/H=3.0$  (pattern 4); (e)  $B/H=4.0$  (pattern 5); (f)  $B/H=7.0$  (pattern 6).  $\alpha_{rms}$  = rms value of angular displacement of the prism,  $f_v$  = vortex shedding frequency,  $f_c$  = natural frequency of the prism,  $U_r$  = reduced velocity. See Fig. 6 for flow visualization patterns with change in  $U_r$ .

occur. The LSTF and VE are convergent vibrations, and the HSTF is a divergent vibration. As shown in Fig. 5(e), for prisms with  $B/H$  ratios ranging from 3.7 to 6.0, LSTF and HSTF are generated, but VE was not observed in the present experiments. It seems that VE is not induced in the case of prisms with  $B/H$  ranging from 3.7 to 6.0 because of weak rolling-up of the Kármán vortices. However, it is possible that VE will be induced if a value of  $C_n$  smaller than those used in the present experiments is adopted. Shiraishi and Matsumoto (1983) and Matsumoto (1999) also found such convergent torsional resonance occurring at lower  $U_r$  than that of HSTF. They called this phenomenon ‘one-shear-layer instability type vortex-oscillation’ which is referred to as LSTF in this paper. The onset velocity of this type of instability is estimated by  $U/(f_c B)$  to be  $1.67/n$  ( $n=1.5$ ) (Shiraishi and Matsumoto 1983). However, this type of instability is called LSTF or VE here depending on the characteristics of the flow that induces vibrations of the prisms. Torsional

resonance at near  $U_r=6, 3.5$  and  $4.5$  for  $B/H=2.0, 3.0$  and  $4.0$ , respectively, is called LSTF because not the wake interactions but the interactions of the shear layers or impingement of leading edge vortices contributed to the resonance in these cases. Also, the characteristics of flow patterns for these values of  $B/H$  were different from those for VE at which the wake behind the prism becomes enhanced. On the other hand, Takeuchi and Matsumoto (1992) called such a resonance at lower  $U_r$  for  $B/H=2.0$  ‘motion-induced excitation’. VE occurs when  $B/H$  exceeds  $6.0$ . This is thought to be because the pattern of flow around the prism changes to one in which the shear layer separating from the leading edge of the prism constantly reattaches to the side surfaces of the prism and then separates again from the trailing edge of the prism, resulting in the generation of Kármán vortices. Some LSTF is observed when  $B/H$  exceeds  $6.0$ , but LSTF is not generated when  $B/H$  exceeded  $8.0$  because there is no alternating rolling-up of the shear layer separating from the leading edges.

Fig. 5 also shows the frequency of vortex shedding of the prism in each pattern. The axis of the ordinate  $f_v/f_c$  shows the ratio of vortex shedding frequency  $f_v$  to natural frequency of the prism  $f_c$ . As is clearly seen from the results, the vortex shedding frequency is synchronized with the natural frequency of the prism when flow-induced vibrations occur. Table 2 shows patterns of response characteristics, which differ depending on the width-to-depth ratio of the prism. As mentioned above, the response characteristics of torsional vibration generated in the rectangular prism could be classified into six patterns depending on the width-to-depth ratio.

Table 2 Classification of generated flow-induced vibration with change in  $B/H$  (○ : occurrence, – : no occurrence)

Pattern	Prism of $B/H$	Vortex excitation	Low-speed torsion flutter	High-speed torsion flutter
1	$B/H < 1.2$	○ (convergence)	–	–
2	$1.2 \leq B/H < 1.7$	○ (divergence)	–	–
3	$1.7 \leq B/H < 2.7$	–	○ (divergence)	○ (divergence)
4	$2.7 \leq B/H < 3.7$	○ (convergence)	○ (convergence)	○ (divergence)
5	$3.7 \leq B/H < 6.0$	–	○ (divergence)	○ (divergence)
6	$B/H \geq 6.0$	○ (convergence)	–	○ (divergence)

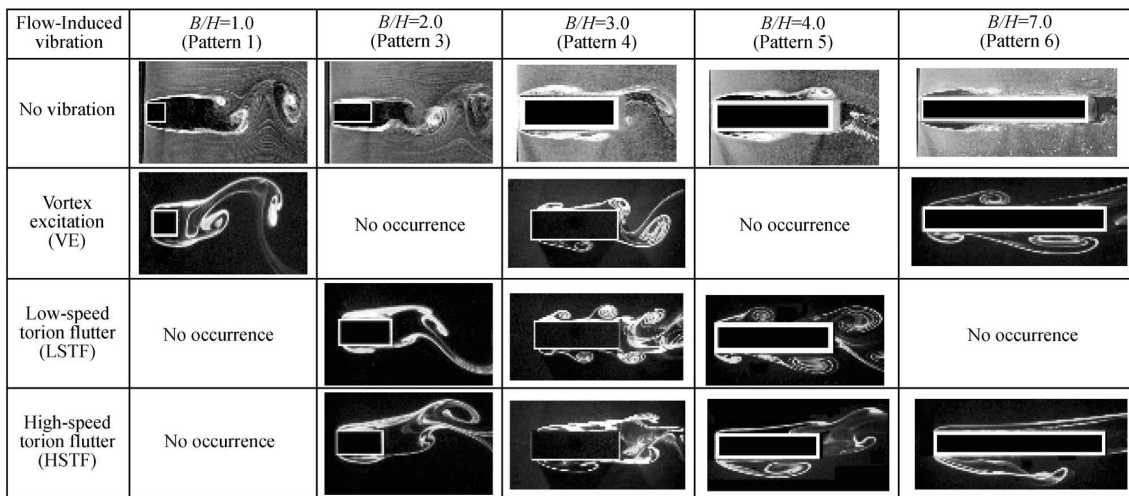


Fig. 6 Visualized flow patterns during the occurrence of flow-induced vibrations of rectangular prisms

Fig. 6 shows the visualized flow patterns during the occurrence of flow-induced vibrations of the prism for  $B/H=1.0, 2.0, 3.0, 4.0$  and  $7.0$ , the response characteristics of which have been described above. Results for prisms with  $B/H$  ratios ranging from  $1.2$  to  $1.6$  that belong to pattern 2 are not shown in Fig. 6 because pattern 2 is not substantially different from pattern 1 except that VE becomes divergent or convergent based on the difference in  $C_n$ . The flow patterns when there is no vibration are also shown for comparison. In the case of a prism with  $B/H=1.0$  that belongs to pattern 1, in which only VE occurs, the shear layer separating from the leading edge does not reattach to the side surfaces but rolls up behind the prism, generating Kármán vortices. In this case, only VE induced by Kármán vortices occurs. Next, in the case of a prism with  $B/H=2.0$  belonging to pattern 3 in which both LSTF and the HSTF occur, the rolling-up of the shear layer under the conditions of both LSTF and the HSTF is quite different. That is in the case of the LSTF, the shear layers separating from the leading edges reattach alternately to the side surfaces. In the case of HSTF, the shear layers do not reattach to the side surfaces but roll up behind the prism. When HSTF occurs, the alternating rolling-up of the shear layers give rise to large fluctuating pressures acting on the side surfaces of the prism. The moment based on these fluctuating pressures acts as an excitation force on the prism, resulting in divergence of the HSTF. In the case of a prism with  $B/H=3.0$  belonging to pattern 4 in which LSTF, VE and HSTF all occur, the shear layers separating from the leading edges cause the generation of impinging leading-edge vortices on the side surfaces of the prism, and then the LSTF is caused by fluctuating pressures due to downward movement of the impinging leading-edge vortices along the side surfaces. When VE occurs, Kármán vortices are generated in synchronization with generation of impinging leading-edge vortices. When HSTF occurs, the shear layers do not reattach to the side surfaces of the prism but roll up behind the prism. This rolling-up of the separated shear layers result in the occurrence of HSTF. In the case of a prism with  $B/H=4.0$  belonging to pattern 5 in which LSTF and HSTF occur, impinging leading-edge vortices are generated when LSTF occurs and alternating rolling-up of the separated shear layers without reattaching on the side surfaces occur when HSTF occurs. These cause the occurrence of LSTF and the HSTF. However, the occurrence of VE is not obvious in pattern 5. This is because the strength of Kármán vortices, which are quite far behind the prism, is not sufficient to cause VE. Finally, in the case of a prism with  $B/H=7.0$  belonging to pattern 6, VE and HSTF occur. However, LSTF is not generated because there is no alternating rolling-up of the shear layer separating from the leading edge.

Fig. 7 shows power spectra of fluctuating velocities in wakes behind rectangular prisms with  $B/H$  ratios of  $1.0, 1.2, 2.0, 3.0, 4.0$  and  $7.0$  corresponding to each pattern shown in Fig. 5. The ratios  $f_v/f_c$  and  $f_v/f_n$  shown in each figure are the ratios of natural vibration frequency of the prism ( $f_c$ ) and natural vortex shedding frequency ( $f_n$ ) to vortex shedding frequency ( $f_v$ ), respectively. As is clearly shown in the figure, vortex shedding occurs in synchronization with the natural vibration frequency of the prism when any type of flow-induced vibration is generated. Also, in the case of prisms with  $B/H=1.0$  and  $1.2$ , in which only VE occurs, the energy level of fluctuating velocity in the wake when vortex shedding frequency is synchronized with natural vibration frequency of the prism is almost the same as that when no flow-induced vibrations are generated. This suggests that even if flow-induced vibrations occur on prisms with relatively small width-to-depth ratios, the intensity of the rolling-up of wake vortices is not greatly increased. However, for prisms with other  $B/H$  ratios, the energy level of the fluctuating velocity in the wake when flow-induced vibration of any type occurs is greater than that when flow-induced vibrations do not occur. The energy level of the fluctuating velocity in the wake is particularly high when HSTF is generated. Thus, when flow-induced vibrations are generated, it seems that the intensity of the rolling-up of wake vortices is greatly increased.

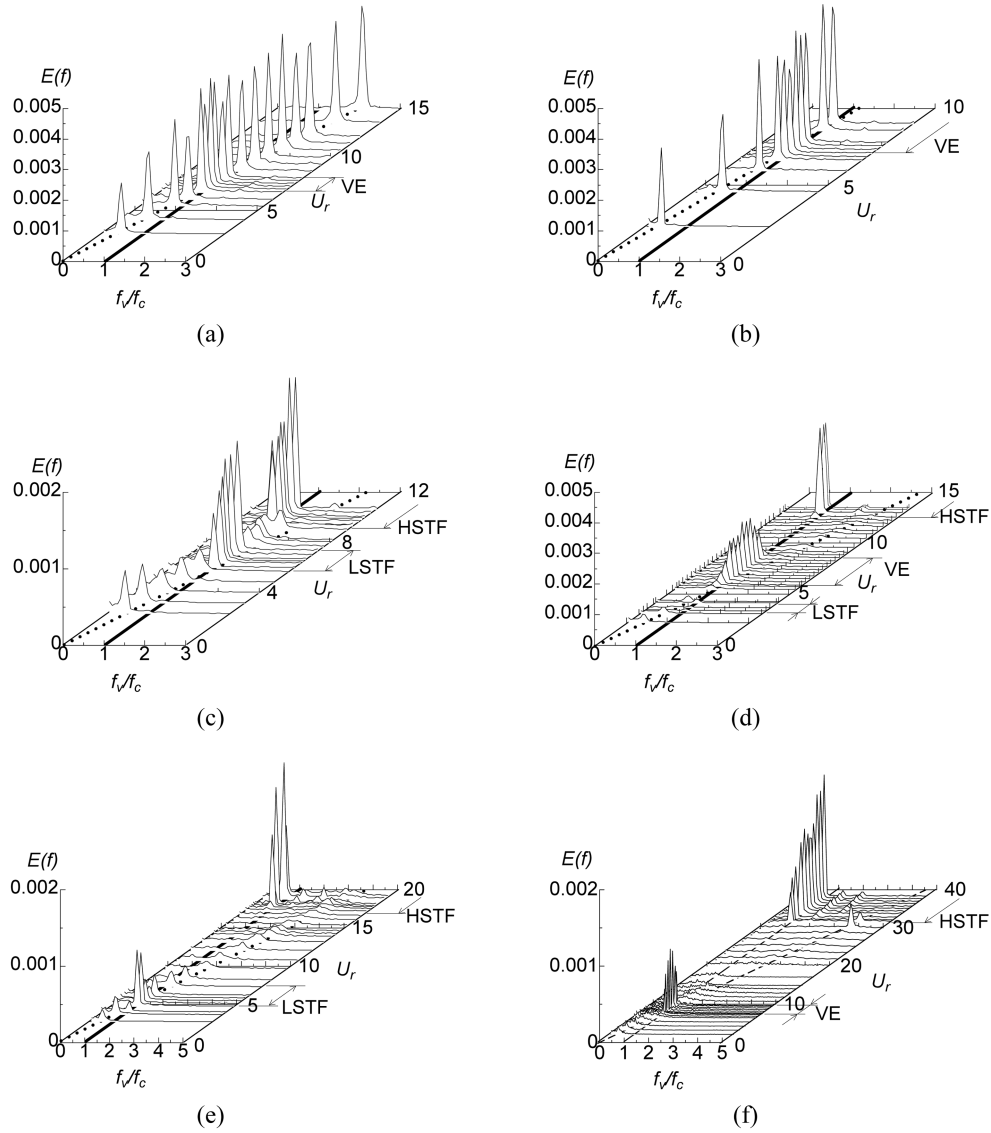


Fig. 7 Power spectra of fluctuating velocity in the wake behind rectangular prism: VE, vortex excitation; LSTF, low-speed torsion flutter; HSTF, high-speed torsion flutter; ---,  $f_v/f_c = 1.0$ ; ...,  $f_v/f_n = 1.0$ ; (a)  $B/H=1.0$  (pattern 1); (b)  $B/H=1.2$  (pattern 2); (c)  $B/H=2.0$  (pattern 3); (d)  $B/H=3.0$  (pattern 4); (e)  $B/H=4.0$  (pattern 5); (f)  $B/H=7.0$  (pattern 6)

#### 4.2. Characteristics of torsional vibration of prisms in response to change in $C_n$

The characteristics of torsional vibrations of prisms in response to changes in the reduced mass-damping factor  $C_n$  are shown in Figs. 8(a)~(f). These results are presented for  $B/H=1.0, 1.2, 2.0, 3.0, 4.0$  and  $7.0$ , which are represented for each flow-induced vibration as mentioned in section 4.1. As can be seen in the figures, LSTF and VE, which are limited vibrations become smaller with increase in  $C_n$  and do not appear when  $C_n$  has reached a certain value. The notable point here is

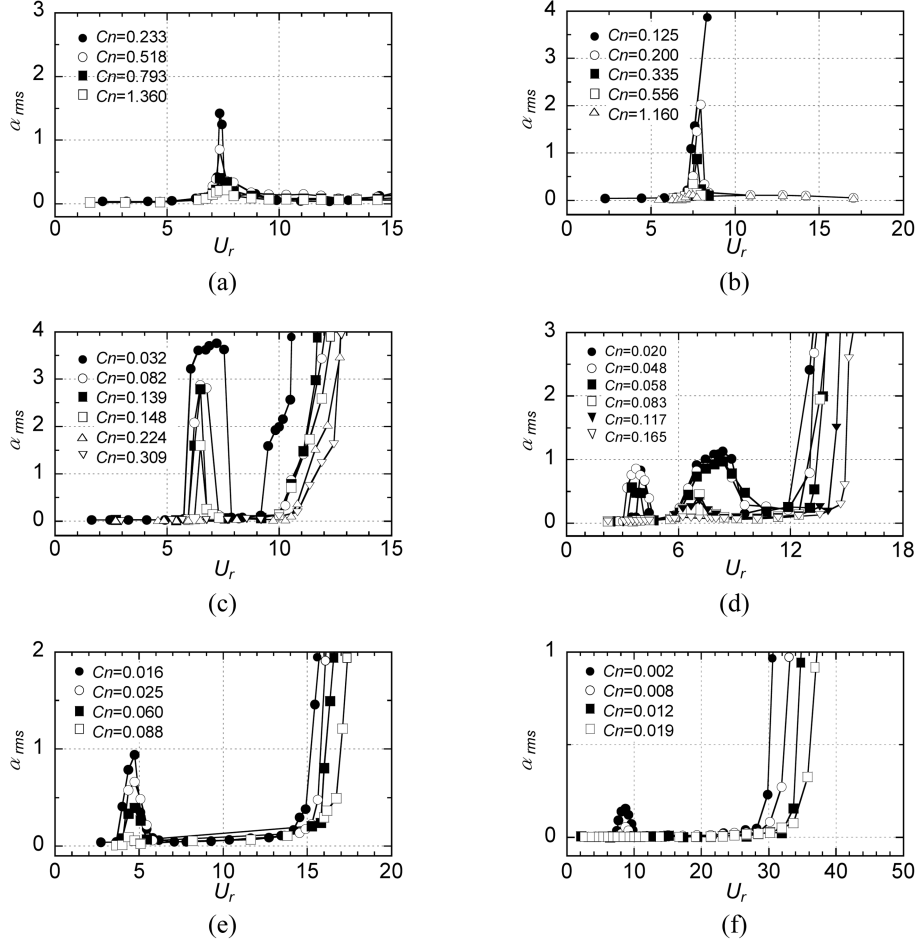


Fig. 8 Characteristics of rotary oscillation of prisms in response to change in  $Cn$ : (a)  $B/H=1.0$  (pattern 1); (b)  $B/H=1.2$  (pattern 2); (c)  $B/H=2.0$  (pattern 3); (d)  $B/H=3.0$  (pattern 4); (e)  $B/H=4.0$  (pattern 5); (f)  $B/H=7.0$  (pattern 6)

that flow-induced vibrations, which are divergent for the  $B/H$  range of 1.2~1.6, are suppressed by increasing the value of  $Cn$ , because the VE in this  $B/H$  range simply changes from convergent to divergent vibration when the value of  $Cn$  is small. On the other hand, the generation of HSTF, which is a divergent vibration, is not suppressed by increasing the value of  $Cn$ . However, the reduced velocity  $U_r$  at which HSTF is generated becomes greater as  $Cn$  increases.

The occurrence of the abovementioned LSTF and VE can be suppressed by increasing  $Cn$ . Fig. 9 shows the values of  $Cn$  required to suppress the occurrence of VE and the LSTF. The occurrence of VE and LSTF can be completely suppressed by increasing  $Cn$  to a level greater than the value calculated by using the following equation:

$$Cn \geq 1.485 \times (B/H)^{-2.184} \quad (5)$$

#### 4.3. Mechanism by which flow-induced vibrations are generated

Flow-induced vibrations of a rectangular prism are strongly dependent on the behavior of rolling-

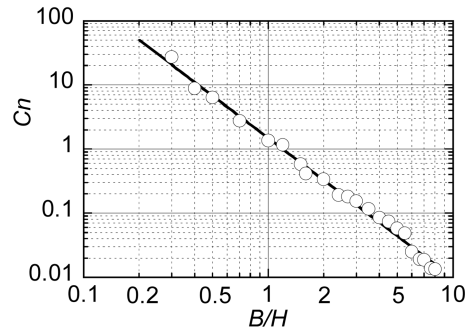
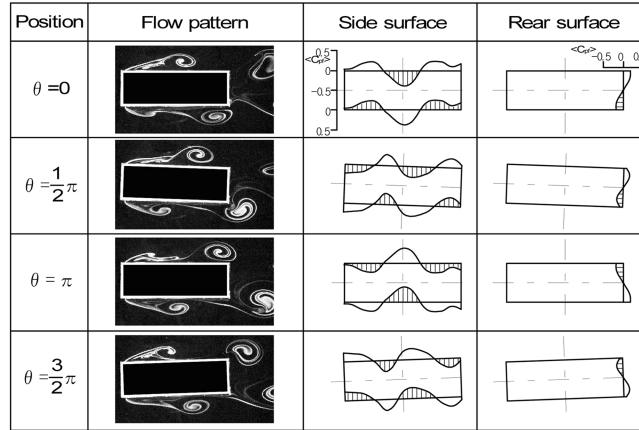


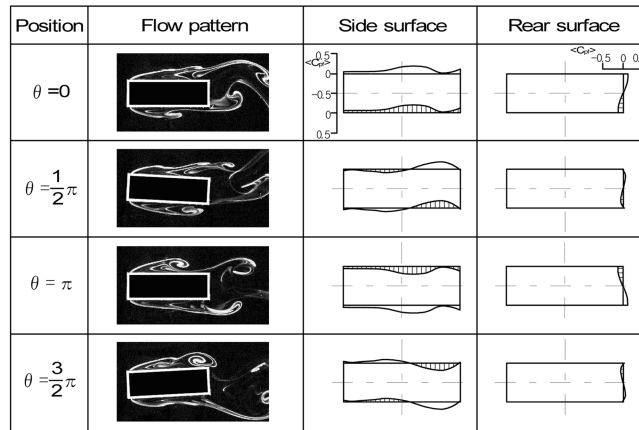
Fig. 9 Values of  $C_n$  required to suppress both low-speed torsion flutter and vortex excitation

up of shear layers, impinging leading-edge vortices on the side surfaces of the prism, and wake vortices. Thus, the mechanisms by which LSTF, VE and HSTF are generated can be clarified by investigating the behavior of these. In this section, the mechanisms by which LSTF, VE and HSTF are generated are examined in the case of a rectangular prism with a  $B/H$  ratio of 3.0, in which three types of flow-induced vibrations occur. Fig. 10 shows the behavior of the shear layers separating from the leading edges of the prism and the distributions of fluctuating pressure acting on the surfaces of the prism when these three types of flow-induced vibrations occur. The results shown in Fig. 10 are concerned with LSTF ( $U_r=3.6$ ), VE ( $U_r=8.1$ ) and HSTF ( $U_r=14.3$ ) (see also Fig. 5(d)) and were obtained from forced-vibration tests. The angular displacements used in the forced-vibration tests were equivalent to those used in the free-vibration tests for which results are shown in Fig. 5(d), i.e.,  $1^\circ$  for LSTF,  $1.5^\circ$  for VE and  $5^\circ$  for HSTF. The flow patterns are shown for each phase with one period of a vibration divided into four equal parts. In the case of LSTF, impinging leading-edge vortices are formed on the side surfaces of the prism, and the position where the fluctuating pressure is negative corresponds to that of the impinging leading-edge vortex (Tang and Rockwell 1983, Gursul and Rockwell 1990). As shown in the figures, the shear layers impinge strongly just from the leading edge, and with regard to angular position of the prism, pressure changes from a high positive value to a high negative value and vice versa, mainly on the front part (leading edge to the midpoint) of each of the side surfaces. The fluctuating pressures are generated due to downward movement of the impinging leading-edge vortices along the side surfaces. Therefore, it can be concluded that LSTF is induced by impinging leading-edge vortices formed on the side surfaces and is mainly due to higher fluctuation of pressure on the front part of each of the side surfaces. Also, LSTF caused by impinging leading-edge vortices is generated at about half the reduced critical velocity  $U_{rc}$  at which VE is induced. This is because of reattachment of the shear layer separating from the leading edge of the prism to the side surfaces of the prism at a frequency two-times greater than that of generation of wake vortices.

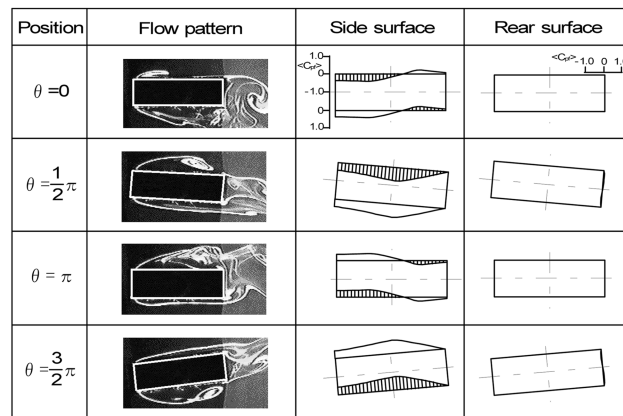
As  $U_r$  increases to 6.0, at which VE occurs, strong impingement of shear layers does not occur from the leading edge but occurs somewhat upstream of the midpoint of each the side surfaces. Thus, greater fluctuation of pressure occurs mainly on the middle part of each of the side surfaces. In this case, rolling up of shear layers occurs in synchronization with the generation of enhanced wake vortices. Also, the shear layers separating from the leading edge reattach alternately to the side surfaces of the prism. This rolling-up of the separated shear layer in synchronization with the generation of wake vortices causes the fluctuating pressures acting on the side surfaces of the prism. These fluctuating pressures are asymmetric with respect to the  $x$ - and  $y$ -axes, which are the central axes of the prism. As a result, a



(a)



(b)



(c)

Fig. 10 Fluctuating pressure distributions on the surfaces of prism and behavior of the separated shear layer when flow-induced vibrations occur in a prism with  $B/H=3.0$ : (a) low-speed torsion flutter ( $U_r=3.6$ ), (b) vortex excitation ( $U_r=8.1$ ) and (c) high-speed torsion flutter ( $U_r=14.3$ )

moment causing torsional vibration of the prism is generated, and VE occurs. Therefore, LSTF is due to interaction of impinging leading edge vortices that impinge from very near the leading edge, and VE is due to the combined effect of interaction of vortices impinging at the middle of each side surface and strong Kármán wake vortices behind the prism. As  $U_r$  increases to 12.3, HSTF is generated and the shear layers separating from the leading edges of the prism do not reattach to the side surfaces of the prism but roll up with a large scale behind the prism. This large-scale rolling-up of the separated shear layers results in the generation of large fluctuating pressures on the side surfaces of the prism. The generated fluctuating pressures are also asymmetric with respect to the central axes of the prism, and a moment causing torsional vibration of the prism is therefore generated.

As described above, three types of flow-induced vibration, i.e., LSTF, VE and HSTF, generated in a rectangular prism depend on the behavior of the shear layers separating from the leading edges of the prism. Thus, it should be possible to prevent all of these flow-induced vibrations by preventing rolling-up of the shear layers separating from the leading edges of the prism and by making the distributions of fluctuating pressures acting on the surfaces of the prism as flat as possible. As is described later, control of the flow approaching the prism and prevention of the rolling-up of shear layers are effective measures for realizing the above-stated requirement.

Three types of flow-induced vibration, i.e., VE, LSTF and HSTF, are generated in a prism. It can be determined by the work done by fluid forces whether these flow-induced vibrations converge or diverge. The work done by fluctuating pressure is estimated from the instantaneous pressure profile on the surfaces for a complete rotation of the prism. The instantaneous pressure profile on the surfaces of the prism is obtained by a phase-averaged technique. The work  $W$  done by fluid forces is estimated on a prism with width-to-depth ratio of  $B/H=3.0$  in which three types of flow-induced vibration (LSTF, VE and HSTF) occur. The work  $W$  done by fluctuating fluid forces for one cycle of torsional vibration is estimated by fluctuating moment  $C_{Mf}$  and angular displacement  $\alpha$  as follows:

$$W = \int_{-\alpha}^{\alpha} C_{Mf}(\theta) \cdot d\alpha \quad (6)$$

The fluctuating moment  $C_{Mf}(\theta)$  in Eq. (6) is estimated by the following equation:

$$\begin{aligned} C_{Mf}(\theta) = & \frac{1}{B^2} \int_{-B/2}^{B/2} \{ [\langle C_{pf}(\theta, x_s) \rangle \cdot x_s]_{Upper} + [\langle C_{pf}(\theta, x_s) \rangle \cdot c_s]_{Lower} \} dx \\ & + \frac{1}{H^2} \int_{-H/2}^{H/2} \{ [\langle C_{pf}(\theta, y_s) \rangle \cdot y_s]_{Front} + [\langle C_{pf}(\theta, y_s) \rangle \cdot y_s]_{Rear} \} dy \end{aligned} \quad (7)$$

where  $\langle C_{pf} \rangle = [1/N \cdot \sum p_f / (0.5\rho U^2)]$ ,  $N$ : ensemble-averaged number] is the ensemble-averaged fluctuating pressure coefficient,  $x_s$  and  $y_s$  are positions of the surface, and  $\theta$  is each phase which is divided one cycle of the oscillation by number of partitions.

Fig. 11 shows the values of work  $W$  estimated by Eq. (6) for a prism with  $B/H$  ratio of 3.0.  $W$  is also estimated for a prism that is forcedly vibrated with angular displacement obtained by the free-vibration test. These angular displacements show one-to-one correspondence shown in Fig. 5(d).  $W$  in the region in which VE and LSTF occur becomes positive over the whole range of values of  $U_r$ . Also,  $W$  increases until the angular displacement attains a maximum value and then it decreases beyond the maximum value. Therefore, LSTF and VE become convergent without diverging. Fig. 12 shows the values of  $W$  when a prism with  $B/H=3.0$  is forcedly vibrated with the angular displacement  $5^\circ$ .  $W$  in the region in which VE and LSTF occur becomes negative. Accordingly, it can be understood that VE and LSTF

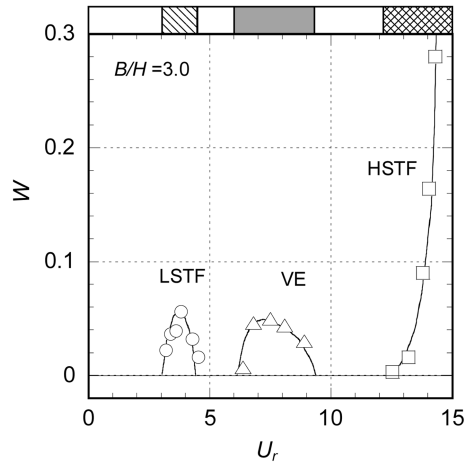


Fig. 11 Work done by fluctuating moment for a prism with  $B/H=3.0$  when the prism is forcedly vibrated with the angular displacement obtained by a free-vibration test:  $\square$ , LSTF;  $\blacksquare$ , VE;  $\boxtimes$ , HSTF

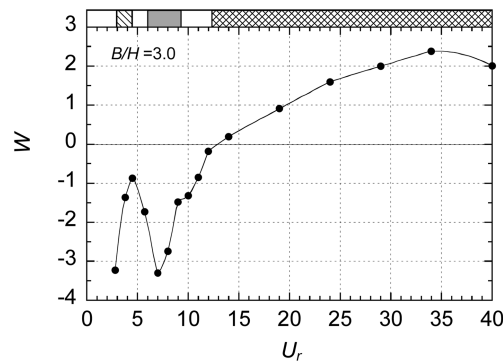


Fig. 12 Work done by fluctuating moment for a prism with  $B/H=3.0$  when the prism is forcedly vibrated with the angular displacement  $\alpha=5^\circ$ :  $\square$ , LSTF;  $\blacksquare$ , VE;  $\boxtimes$ , HSTF

with large amplitude do not occur. Washizu, *et al.* (1976) also reported that the magnitude of an unsteady aerodynamic pitching moment is dependent on amplitude. For example, for  $B/H=4.0$ , in the relatively lower wind velocity regions where LSTF and VE occur, when the amplitude is large, its magnitude shows a large negative value and then  $W$  also shows a large negative value. However, the results obtained by Washizu, *et al.* suggest that  $W$  decreases with decrease in amplitude and then  $W$  changes from a negative value to a positive value. Therefore, it can be concluded that the magnitudes of the amplitudes of VE and LSTF are considerably small. On the other hand,  $W$  in the region in which HSTF occurs becomes positive over the whole range of values of  $U_r$ . The vibration becomes divergent without converging. Therefore, it can be seen that the work done by fluctuating fluid forces corresponds to the convergence or divergence of flow-induced vibrations of the prism.

#### 4.4. Suppression of flow-induced vibrations

As mentioned above, the types of flow-induced vibration generated in a rectangular prism depend on the

behavior of the shear layers separating from the leading edges of the prism. LSTF occurs under the condition of generation of impinging leading-edge vortices caused by alternating rolling-up of the separated shear layers, VE occurs under the condition of alternating rolling-up of the separated shear layers in synchronization with the generation of Kármán vortices, and HSTF occurs under the condition of large-scale rolling-up of the separated shear layers behind the prism without reattachment of the shear layers to the side surfaces of the prism. Thus, it can be conjectured that it is possible to suppress the generation of these three types of flow-induced vibration in a rectangular prism by preventing rolling-up of the shear layers separating from the leading edges of the prism. It has been demonstrated that the generation of fluctuating fluid forces and the wake vortices of a rectangular prism can be almost completely suppressed by placing a small normal plate upstream of the prism (Sakamoto, *et al.* 2002). This is because the small normal plate causes turbulent diffusion of the shear layers separating from the leading edges of the prism, thus preventing rolling-up of the separated shear layers. Consequently, it is thought that the generation of flow-induced vibrations of a rectangular prism can be suppressed by placing a small normal plate upstream of the prism since the generation of flow-induced vibrations is induced by the rolling-up of the separated shear layers. Also, since VE occurs under the condition of alternating rolling-up of the separated shear layer in synchronization with the generation of Kármán vortices, it should be possible to prevent the occurrence of VE by suppressing the generation of Kármán vortices.

In this study, we therefore attempted to suppress the generation of flow-induced vibrations of a rectangular prism by the following two methods: placement of a normal plate upstream of the prism for suppression of rolling-up of the separated shear layers and placement of a splitter plate downstream of the prism for suppression of the generation of Kármán vortices. For suppression of the generation of flow-induced vibrations, a normal plate with a width of 30 mm ( $w/H=0.3$ ) was placed upstream of the prism at a position of  $s/H=1.25$  from the prism. The evaluation of the width and the installing position of the normal plate have variously changed for rectangular prisms with various width-to-depth ratios  $B/H$ . As a result, it was found that the generation of flow-induced vibration of all prisms can be most suppressed in the case of  $w/H=0.3$  and  $s/H=1.25$ . These conditions were used for subsequent experiments. The length of the splitter plate ( $L/H$ ) used in the experiments was determined on the basis of the results regarding suppression of the generation of Kármán vortices by placement of a splitter plates reported by Bearman (1965).

Fig. 13 shows the response characteristics of rectangular prisms with  $B/H$  ratios of 1.0, 1.2, 2.0, 3.0, 4.0 and 7.0 when a normal plate is placed upstream or when a splitter plate is placed downstream of the prism. In the case of prisms with  $B/H$  ratios of 1.0 and 1.2, in which only VE occurs, flow-induced vibrations are completely suppressed due to prevention of the rolling-up of the shear layers separating from the leading edges of the prism by the use of the splitter plate. However, in the case of placement of the normal plate upstream of the prism, since the shear layers separating from the leading edges of the prism reattach alternately to the side surfaces of the prism and then separate again from the trailing edges of the prism resulting in the generation of the wake vortices, VE occurs at a value of  $U_r$  that differs from the reduced critical velocity  $U_{rc}$ , though the amplitude of the excitation is very small. Figs. 14(a) and (b) show power spectra of fluctuating velocity in the wake behind prisms when the normal plate was placed upstream of the prism with  $B/H$  ratios of 1.0 and 1.5, respectively. Although the energy level is very small, there is a clear peak in each spectrum, indicating that wake vortices are generated. In the case of a prism with a  $B/H$  ratio of 2.0, in which LSTF and HSTF occur, the generation of LSTF is completely suppressed by the use of the splitter plate and the normal plate, respectively. It is notable that the placement of the normal plate upstream of the prism completely suppresses the generation of HSTF, which was not suppressed by

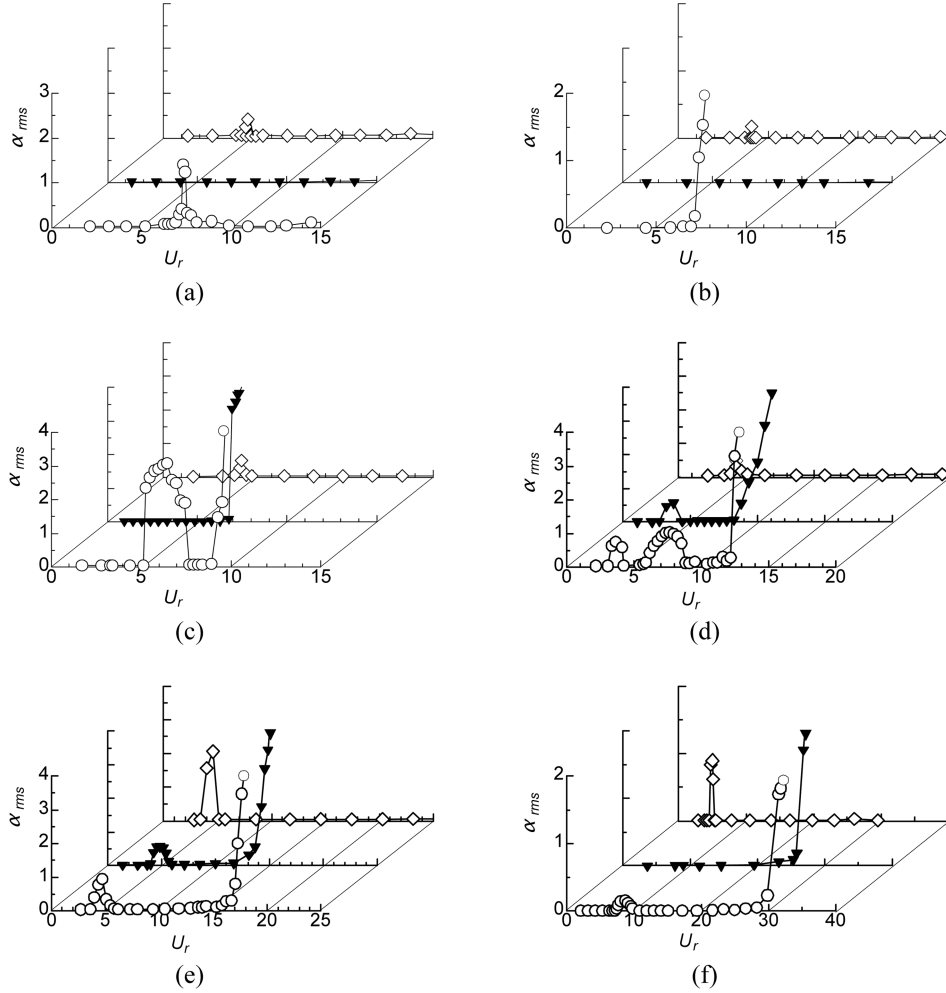


Fig. 13 Response characteristics of rectangular prisms when a normal plate and splitter plate are placed upstream and downstream of the prism, respectively;  $\circ$ , plain prism;  $\blacktriangledown$ , prism with splitter plate;  $\diamond$ , prism with normal plate; (a)  $B/H=1.0$  (pattern 1); (b)  $B/H=1.2$  (pattern 2); (c)  $B/H=2.0$  (pattern 3); (d)  $B/H=3.0$  (pattern 4); (e)  $B/H=4.0$  (pattern 5); (f)  $B/H=7.0$  (pattern 6)

increasing the reduced mass-damping factor  $C_n$  (§4.2). However, as indicated by the spectrum shown in Fig. 14(c), wake vortices are generated when a normal plate is placed. The wake vortices cause the generation of VE at a value of  $U_r$ , which differs from the critical reduced velocity  $U_{rc}$ . In the case of a prism with a  $B/H$  ratio of 3.0, in which all of the three types of flow-induced vibration are generated, the use of the splitter plate results in suppression of only the generation of VE, whereas the use of the normal plate results in complete suppression of the generation of both LSTF and HSTF. However, as indicated by the spectrum shown in Fig. 14(d), wake vortices are generated when the normal plate is placed, and VE therefore occurs. In the case of a prism with a  $B/H$  ratio of 4.0, in which both LSTF and HSTF occur, two types of flow-induced vibration are completely suppressed by placement of the normal plate upstream of the prism. However, VE occurs due to the generation of wake vortices, as indicated by the power spectrum shown in Fig. 14(e). The resonance

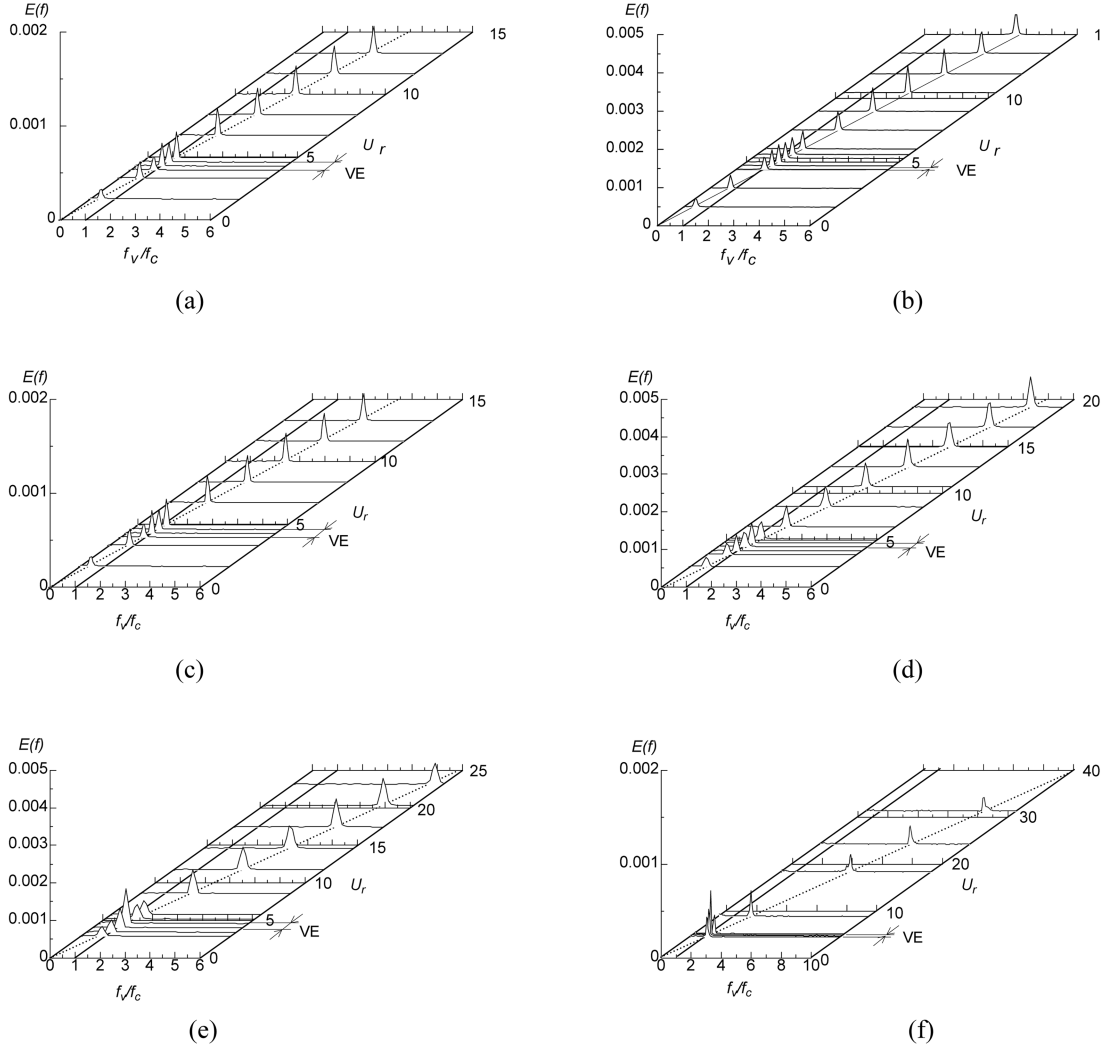


Fig. 14 Power spectra of fluctuating velocity in the wake behind a rectangular prism when a normal plate is placed upstream of the prism: VE, vortex excitation; —,  $f_v/f_c = 1.0$ ; ----,  $f_v/f_n = 1.0$ ; (a)  $B/H = 1.0$ , (b)  $B/H = 1.5$ , (c)  $B/H = 2.0$ , (d)  $B/H = 3.0$ , (e)  $B/H = 4.0$  and (f)  $B/H = 7.0$ .

at  $U_r = 4$  for the plain prism is LSTF; however, at the same  $U_r$ , another resonance occurs when a normal plate is placed upstream of the prism. Due to placement of a normal plate, critical reduced velocity for the prism with a normal plate is different from that of the plain prism, and by chance it was  $U_r = 4$ . Thus, the resonance at  $U_r = 4$  for the prism with a normal plate is VE at the critical reduced velocity. In the case of a prism with a  $B/H$  ratio of 7.0, in which VE and HSTF occur, the generation of HSTF is completely suppressed when a normal plate is placed upstream of the prism as was found in the case of other width-to-depth ratios.

Fig. 15 shows the visualized flow patterns of the rectangular prisms with  $B/H$  ratios of 1.0, 1.5, 2.0, 3.0, 4.0 and 6.0 when a normal plate is placed upstream of the prism. Also, the visualized flow patterns of the plain rectangular prisms show to compare those of the rectangular prisms having the

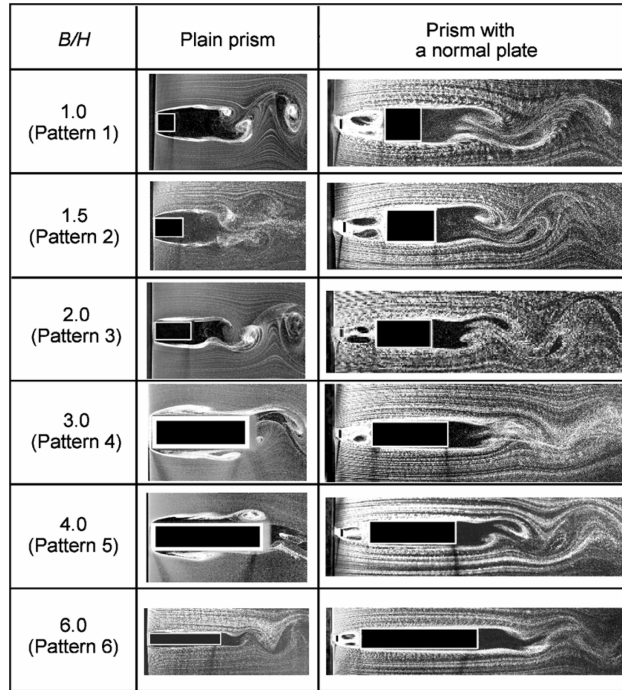
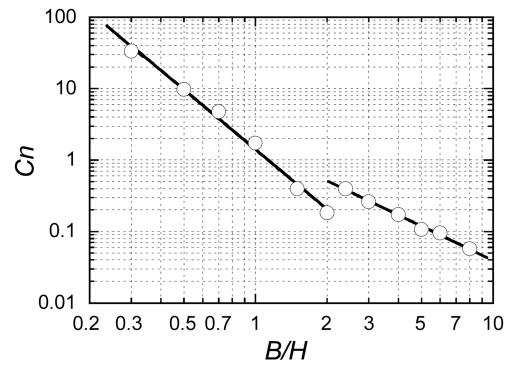


Fig. 15 Visualized flow patterns of rectangular prism with a normal plate

Fig. 16 Values of  $C_n$  required to suppress vortex excitation when a normal plate is placed

normal plate. The results are shown as a representative pattern in each of the response characteristics, which is classified into six patterns. In the case of prisms with  $B/H$  ratios of 1.0 and 1.5, in which only VE occurs, the rolling-up of the shear layers separating from the leading edges of the prism is completely prevented by placing the normal plate. However, the shear layers separating from the leading edges of the prism which reattach to the side surfaces separate again from the trailing edges, and Kármán vortices are formed with the different shedding frequency. As a result, the Kármán vortices cause the generation of VE at a value of  $U_c$ , which differs from that of the plain prism. Furthermore, in all cases of the prism with  $B/H$  ratios of 2.0, 3.0, 4.0 and 6.0, the rolling-up of the separating shear layers from the leading edges of the prism is prevented. Therefore the generation

of LSTF, VE and HSTF based on the rolling-up the separating shear layers from the leading edges of the prism are completely suppressed. However, since the Kármán vortices are clearly formed, the generation of VE occurs at the position of  $U_r$ , which is different from that of the plain prism.

As mentioned above, a normal plate placed upstream of the prism is effective for suppressing LSTF and HSTF. However, VE of small amplitude is generated. Since the generated VE is a limited vibration, it can be suppressed by increasing the reduced mass-damping factor  $Cn$ . Fig. 16 shows the required values of  $Cn$  to suppress VE. Therefore, it seems that VE can be completely suppressed by increasing  $Cn$  to a level greater than the value calculated by using the following equation:

$$\left. \begin{aligned} Cn &\geq 1.42 \times (B/H)^{-2.78} \quad (B/H \leq 2.0) \\ Cn &\geq 1.54 \times (B/H)^{-1.59} \quad (B/H > 2.0) \end{aligned} \right\} \quad (8)$$

## 5. Conclusions

Flow-induced torsional vibrations generated in rectangular prisms with various width-to-depth ratios were investigated in the present study. The response characteristics and the generation mechanism of flow-induced torsional vibration of elastically mounted prisms, allowing only the torsional component of vibration, were examined in detail by using free-vibration and forced-vibration tests. An effective method for suppressing flow-induced vibrations of rectangular prisms was established. The results led to the following conclusions:

- (1) The results of free-vibration tests using plain rectangular prisms in a steady flow show that there are three types of flow-induced vibration, i.e., low-speed torsional flutter, vortex excitation and high-speed torsional flutter.
- (2) The generation of low-speed torsional flutter and vortex excitation is completely suppressed by adopting large values of the reduced mass-damping factor  $Cn$ . However, high-speed torsional flutter occurs regardless of  $Cn$ .
- (3) Observation of the behavior of shear layers separating from the leading edges of the prism indicates that flow-induced vibrations occur due to change in fluctuating pressure acting on the surfaces of the prism.
- (4) Whether the generating flow-induced torsional vibrations become divergent or convergent can be determined from the work done, calculated from surface pressures acting on side surfaces of the prism.
- (5) A normal plate placed upstream of the rectangular prism can suppress the generation of low-speed and high-speed torsional flutters, and a splitter plate placed downstream of the rectangular prism can suppress the generation of vortex excitation.
- (6) The generation of vortex excitation when a normal plate is placed upstream of the prism can be completely suppressed by increasing the value of  $Cn$  from the threshold value.

## References

- Bearman, P.W. (1965), "Investigation of the flow behind a two-dimensional model with a blunt trailing edge and fitted with splitter plate", *J. Fluid Mech.*, **21**-2, 241-255.
- Deniz, S. and Staubli, T. (1997), "Oscillating rectangular and octagonal profiles: Interaction of leading- and trailing-edge vortex formation", *J. Fluids Struct.*, **11**, 3-31.
- Gursul, I. and Rockwell, D. (1990), "Vortex street impinging upon an elliptical leading edge", *J. Fluid Mech.*,

- 211**, 211-242.
- Itoh, Y. and Tamura, T. (2002), "The role of separated shear layers in unstable oscillations of a rectangular cylinder around a resonant velocity", *J. Wind Eng. Ind. Aerodyn.*, **90**, 377-394.
- Komatsu, S. and Kobayashi, H. (1980), "Vortex-induced oscillation of bluff cylinders", *J. Wind Eng. Ind. Aerodyn.*, **6**, 335-362.
- Leonard, A. and Roshko, A. (2001), "Aspects of flow-induced vibration", *J. Fluids Struct.*, **15**, 415-425.
- Matsumoto, M., Kobayashi, K. and Shirato, H. (1996), "The influence of aerodynamic derivatives on flutter", *J. Wind Ind. Eng. Aerodyn.*, **60**, 227-239.
- Matsumoto, M., Daito, Y., Yoshizumi, F., Ichikawa, Y. and Yabutani, T. (1997), "Torsional flutter of bluff bodies", *J. Wind Ind. Eng. Aerodyn.*, **69-71**, 871-882.
- Matsumoto, M. (1999), "Vortex shedding of bluff bodies: A review", *J. Fluids Struct.*, **13**, 791-811.
- Mills, R., Sheridan, J. and Hourigan, K. (2003), "Particle image velocimetry and visualization of natural and forced flow around rectangular cylinders", *J. Fluid Mech.*, **478**, 299-323.
- Munshi, S.R., Modi, V.J. and Yokomizo, Y. (1997), "Aerodynamics and dynamics of rectangular prisms with momentum injection", *J. Fluids Struct.*, **11**, 873-892.
- Nakaguchi, Y., Hashimoto, T. and Muto, S. (1968), "An experimental study on aerodynamic drag of rectangular cylinders", *J. Japan Society for Aeronautical and Space Sciences*, **16-168**, 1-5 (in Japanese).
- Nakamura, Y. and Nakashima, M. (1986), "Vortex excitation of prisms with elongated rectangular, H and cross-sections", *J. Fluid Mech.*, **163**, 149-169.
- Nakamura, Y. and Matsukawa, T. (1987), "Vortex excitation of rectangular cylinders with a long side normal to the flow", *J. Fluid Mech.*, **180**, 171-191.
- Nakamura, Y. and Hirata, K. (1994), "The aerodynamic mechanism of galloping", *Transactions of Japan Society for Aeronautical and Space Sciences*, **36-114**, 257-269.
- Naudascher, E., Weske, J.R. and Fey, B. (1981), "Exploratory study on damping of galloping vibrations", *J. Wind Eng. Ind. Aerodyn.*, **8**, 211-222.
- Okajima, A., Sugitani, K. and Mizota, T. (1980), "Strouhal number and base pressure coefficient of rectangular cylinders (The case of a section of a width/height ratio of 1-9)", *Transactions of the Japan Society of Mechanical Engineers*, **B 49-447**, 2551-2558 (in Japanese).
- Otsuki, Y., Washizu, K., Tomizawa, H. and Ohya, A. (1974), "A note on the aeroelastic instability of a prismatic bar with square section", *J. Sound and Vib.*, **34-2**, 233-248.
- Sakamoto, H., Haniu, H. and Kobayashi, K. (1989), "Fluctuating forces acting on rectangular cylinders in uniform flow (On rectangular cylinders with fully separated flow)", *Transactions of the Japan Society of Mechanical Engineers*, **B 55-516**, 2310-2317 (in Japanese).
- Sakamoto, H., Takai, K., Alam, M.M. and Moriya, M. (2002), "Generation mechanism and characteristics of flow-induced vibrations of rectangular prism with various width-to-height ratios", *Proc. of the 5th International Conference on Hydrodynamics, Tainan*, 293-298.
- Shiraishi, Y. and Matsumoto, M. (1983), "On classification of vortex-induced oscillation and its application for bridge structures", *J. Wind Eng. Ind. Aerodyn.*, **14**, 419-430.
- Takai, K., Sakamoto, H., Alam, M.M. and Moriya, M. (2000), "Suppression and generation mechanism of flow-induced vibrations of a rectangular prism with impinging leading-edge vortices", *Proc. of the 4th International Conference on Hydrodynamics*, **1**, Yokohama, 471-476.
- Takeuchi, T. and Matsumoto, M. (1992), "Aerodynamic response characteristics of rectangular cylinders in tandem arrangement", *J. Wind Ind. Eng. Aerodyn.*, **41-44**, 565-575.
- Tamura, T. and Dias, P.P.N.L. (2003), "Unstable aerodynamic phenomena around the resonant velocity of a rectangular cylinder with small side ratio", *J. Wind Eng. Ind. Aerodyn.*, **91**, 127-138.
- Tang, Y.P. and Rockwell, D. (1983), "Instantaneous pressure fields at a corner associated with vortex impingement", *J. Fluid Mech.*, **126**, 187-204.
- Washizu, K., Ohya, A., Otsuki, Y. and Fuji, K. (1976), "Wind tunnel experiments on the aeroelastic instability of prismatic models with rectangular sections", *Proceedings of the Fourth Symposium on Wind Effects on Structures in Japan*, 191-198.